L-H Transition Dynamics in ITER-Similar Plasmas with Applied n=3 Magnetic Perturbations*

L. Schmitz,[1] M. Kriete,[2] R. Wilcox,[3] Z. Yan,[2] T.L. Rhodes,[1] G.R. McKee,[2] C. Paz-Soldan,[4] L. Zeng,[1] A. Marinoni,[5] P. Gohil,[4] B. Lyons,[4] and C.C. Petty.[4]

[1]*University of California-Los Angeles, Los Angeles, CA 90095-7799, USA*
[2]*University of Wisconsin-Madison, Madison, WI 53706, USA*
[3]*Oak Ridge National Laboratory, Oak Ridge, TN 37831-0117, USA*
[4]*General Atomics, PO Box 85608, San Diego, CA 92186-5608, USA*
[5]*PFSC, Massachusetts Institute of Technology, Cambridge, MA 02139, USA*

In ITER-similar shape (ISS), low rotation plasmas [1] in DIII-D [$\langle n_e \rangle$=1.5-5x10^{19}m^{-3}, B_t=1.9-2T, I_p=1.5MA, q_{95}~3.6, balanced neutral beam injection (NBI)], the L-H threshold power P_{LH} with applied n=3 Resonant Magnetic Perturbations (RMP) [2,3] is found to increase strongly with decreasing collisionality. This is a concern for H-mode access in primarily ECH-heated ITER plasmas since RMP may be applied before the L-H transition in ITER to safely suppress the first ELM. The L-H power threshold increase with RMP is determined by initially accessing H-mode via applying balanced NBI and increasing steps in ECH power at high RMP field (applied via the DIII-D I-coil system consisting of six internal coils above and six coils below the outboard tokamak midplane [2]). NBI and ECH power are then removed to let the plasma return to L-mode. A second L-H transition is induced later in the same shot by applying NBI and stepping up ECH power again to obtain the threshold power with no applied RMP as a reference. Using this method to bracket P_{LH}, a scan of P_{LH} vs. RMP perturbation strength is then obtained via stepping down the I-coil current (RMP perturbation strength) at constant beam and ECH power, as shown in Fig. 1.

Repeating this shot sequence for different plasma densities, P_{LH} has been determined vs. RMP perturbation strength and line-averaged density, as shown in Fig. 2. A clear threshold in perturbation strength is observed [$\delta B_r/B \sim 3\times10^{-4}$ for medium plasma density, Fig. 2(a)]. This threshold is below the optimum RMP field typically required for ELM suppression. For

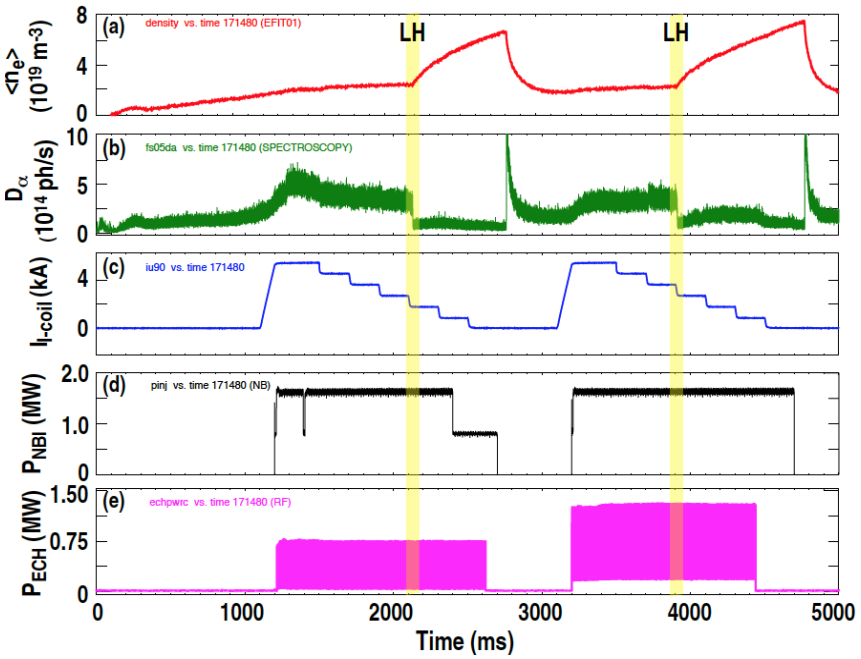

Fig. 1: (a) Line-averaged density, $\langle n_e \rangle$; (b) divertor D_α signal; (c) I-coil current; (d) neutral beam power; (e) Electron cyclotron heating (ECH) power during L-H transition threshold power studies.

comparison, previous work in other devices has shown that edge-resonant n=1 and n=2 fields of $\delta B_r/B \sim 1\text{-}2\times10^{-4}$ can increase P_{LH} (see for example [4,5]). Fig. 2(b) shows that the density dependence of P_{LH} is not very pronounced in these ISS low-rotation plasmas. Without applied RMP, the threshold power is increased with mixed heating (ECH at 30-100% of the total heating power in addition to NBI), compared to pure NBI heating. This increase may result from higher electron thermal loss due to the increased edge electron temperature with ECH [6]. With moderate applied RMP ($\delta B_r/B \sim 3.1\text{-}3.7\times10^{-4}$), the power threshold increases at low density but not at high density in NBI plasmas. A more pronounced increase (~ 40%) is found with mixed heating (added ECH). At high perturbation strength ($\delta B_r/B \sim 4.7\times10^{-4}$), P_{LH} can be doubled compared to the threshold without applied RMP. Here, the absolute increase in power with applied RMP is similar for NBI and for mixed heating.

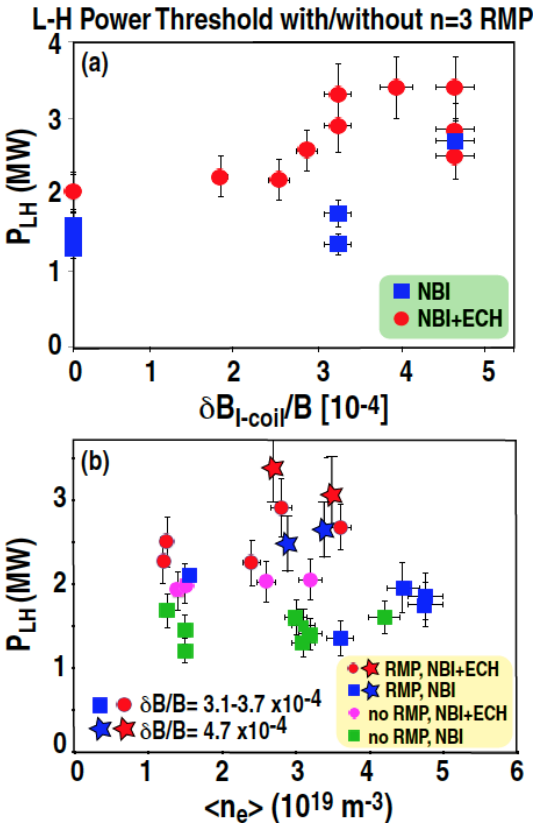

Fig.2: Increase of P_{LH} with n=3 RMP for NBI and mixed heating (NBI+ ECH); (a) vs. RMP perturbation strength; (b) vs. plasma density.

The power threshold data obtained with NBI- and mixed NBI/ECH heating show a clear dependence on normalized edge plasma collisionality ν^* (ρ =0.95, Fig. 3). P_{LH} increases for low collisionality, and the collisionality dependence of P_{LH} is much more pronounced with applied RMP [$P_{LH} \sim (\nu^*)^{-0.3}$] compared to non-RMP reference plasmas [$P_{LH} \sim (\nu^*)^{-0.1}$].

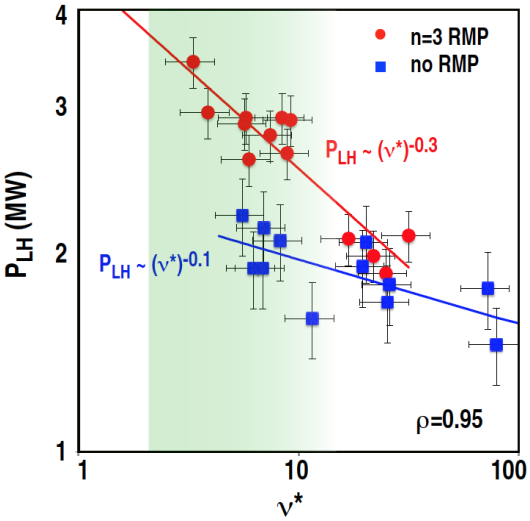

Fig. 3: L-H transition power threshold P_{LH} vs. collisionality ν^* (ρ = 0.95) without and with applied n=3 RMP ($3.3\times10^{-4} \le \delta B/B \le 4.6\times10^{-4}$ The expected ITER L-mode edge collisionality range is shaded.

Characteristic changes in the edge plasma normalized kinetic gradients, the radial electric field, and the edge turbulence properties have been observed with RMP. Non-axisymmetric modifications of the L-mode shear layer with RMP include a substantial local reduction of the E_r well and $\boldsymbol{E\times B}$ shear. Figure 4(a) shows a comparison of the radial electric field, extracted via Doppler Backscattering (DBS [7,8]) from the Doppler shift associated with poloidal turbulence advection. E_r increases primarily due to increasing toroidal edge rotation (DBS data shown for a toroidal angle $\phi_{tor} \sim 50°$. Phase flip experiments have determined that these

changes are most pronounced for flux tubes connecting to high I-coil perturbation field). At high resonant perturbation strength, the E_r well is reduced by more than 50% and E_r can locally reverse (not shown here). With resonant n=3 perturbations, in particular the outboard $\boldsymbol{E\times B}$ shearing rate is locally reduced. Concomitantly, low-wavenumber density fluctuations measured by Beam Emission Spectroscopy (BES) are spatially modulated with applied RMP, and increase substantially in amplitude on field lines connecting to high RMP field [see Fig. 4(b), for a toroidal angle ϕ_{tor} ~137°]. Application of (moderate) non-resonant n=3 magnetic perturbations leads only to small changes in E_r near the boundary and inboard of the maximum negative electric field, and a minor change in the $\boldsymbol{E\times B}$ shear. Turbulence levels are almost unchanged (perhaps slightly reduced) with non-resonant perturbations [Fig. 4(b)]. Correspondingly, the L-H power threshold increases only moderately in this case.

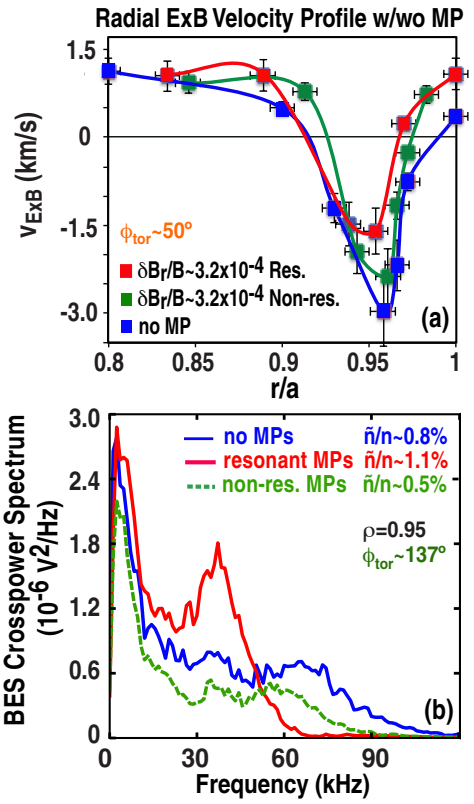

Fig. 4: (a) L-mode electric field well for different RMP perturbation strength (toroidal angle ϕ_{tor} ~50°); (b) the BES density fluctuation spectrum at ϕ_{tor} ~137° increases substantially for resonant perturbations, but is slightly reduced for non-resonant perturbations.

Two-fluid modeling with the M3D-C1 code [9,10] shows that the normalized radial density gradient a/L_n and the normalized electron and ion pressure gradients are toroidally modulated and periodically increased on the outboard midplane with n=3 RMP, at locations that map to maximum outwardly directed radial magnetic field perturbation. Figure 5 shows a contour plot of the normalized plasma density gradient a/L_n (where a is the minor radius and L_n is the density gradient scale length) at the DIII-D outboard midplane vs. major radius R and toroidal angle ϕ_{tor}. Electron temperature contours are indicated as white dashed lines; equidensity contours are marked in blue. Electron temperature contours tend to coincide with flux surface contours due to the low electron inertia, The brightest white dashed contour line approximately indicates the last closed flux surface (LCFS). A toroidal modulation of the normalized radial density gradient of about 20% is observed in this contour plot, peaking inside the separatrix. Experimentally, a/L_n increases locally by a similar amount, as measured via profile reflectometry in phase flip experiments. The normalized electron and ion temperature gradients a/L_{Te}, a/L_{Ti} also increase mildly (not shown here). The divergence of the density and electron temperature contours indicates that ion mass flow can deviate from electron flow, an effect captured only in the two-fluid model. The BES and DBS probing locations, mapped to the tokamak midplane, are indicated in Fig. 5. The increased turbulence level observed via BES at the probing location ϕ_{tor} ~137° is qualitatively consistent with locally increased kinetic gradients. The reduced E_r

well with resonant perturbations is also consistent with a reduced normalized (ion) pressure gradient at ϕ_{tor} ~50° (the mapped DBS location).

The observed increase of P_{LH} at low collisionality [$P_{LH} \sim (\nu^*)^{-0.3}$] is a concern for H-mode access with applied RMP in ITER, and further work is required to determine the underlying physics of this collisionality scaling. The loss of axisymmetry reduces the globally driven (n=0, m=0) ***E×B*** flow in the edge layer (where n,m are the toroidal/poloidal mode numbers). We conjecture that the increase in P_{LH} with RMP results from the combined effects of reduced flow axisymmetry, reduced ***E×B*** shear, and locally enhanced instability drive (via increased normalized kinetic gradients).

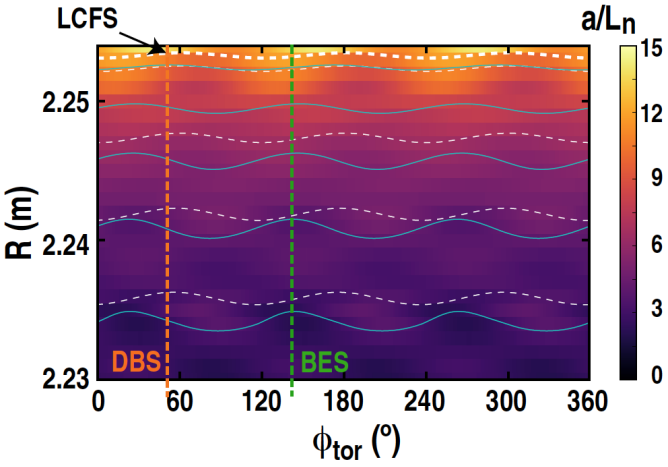

Fig. 5: (a) Outboard midplane contours of the normalized density gradient a/L_n for resonant perturbations ($\delta B_r/B \sim 4.7\times10^{-4}$) vs. toroidal angle ϕ_{tor}; the probing locations of the DBS and BES diagnostics, mapped to the tokamak midplane, are indicated.

It has been proposed theoretically that increased Reynolds stress [11] may be required to initiate the L-H transition with RMP active [12], as the Reynolds stress may be locally counteracted by radial forces related to the RMP field structure [12], and would also likely be less effective globally due to the non-axisymmetric edge topology. Further experimental work and gyrokinetic modeling of the turbulence evolution preceding the transition will be required to determine if the observed threshold increase with applied RMP is related to potential modifications in the Reynolds stress or other edge momentum sources.

[1] T.E. Evans, M.E. Fenstermacher, R.A. Moyer et al. Nucl. Fusion 48 024002 (2008).
[2] T.E. Evans, R.A. Moyer, J.G. Watkins et al. Nucl. Fusion 45 595 (2005).
[3] P. Gohil, T.E. Evans, et al. Nucl. Fusion 51, 030120 (2011).
[4] A.W. Leonard, et al. Nucl. Fusion 31, 1511-1518 (1991).
[5] Y. In et al. Nucl. Fusion 57, 116054 (2017).
[6] F. Ryter et al. Nucl. Fusion **54** 083003 (2014).
[7] J.C. Hillesheim, W.A. Peebles, T.L. Rhodes, L. Schmitz, et al. Rev. Sci. Instr. 81 10D907 (2010).
[8] W.A. Peebles, T.L. Rhodes, J.C. Hillesheim, L. Zeng, and C. Wannberg, Rev. Sci. Instr. 81 10D902 (2010).
[9] N.M. Ferraro, Phys. Plasmas **19** 056105 (2012).
[10] R.S. Wilcox et al. Phys. Plasmas **25** 056108 (2018); R.S. Wilcox et al. Nucl. Fusion **57** 116003 (2017).
[11] Z.Yan et al. Nucl. Fusion **57** 126015 (2017); Z. Yan, et al. Phys Rev. Lett**. 107** 055004 (2014).
[12] M. Leconte et al. Nucl. Fusion **54** 013004 (2014); G. Choi and T.S. Hahm, Nucl. Fusion **58** 026001 (2018).

*This material is based upon work supported by the U.S. Department of Energy, Office of Science, Office of Fusion Energy Sciences, using the DIII-D National Fusion Facility, a DOE Office of Science user facility, under Awards DE-FG02-08ER54984, DE-FG02-89ER53296, DE-FG02-08ER 54999, and DE-FC02-04ER54698.DIII-D data shown in this paper can be obtained in digital format by following the links at https://fusion.gat.com/global/D3D_DMP.Disclaimer-This report was prepared as an account of work sponsored by an agency of the United States Government. Neither the United States Government nor any agency thereof, nor any of their employees, makes any warranty, express or implied, or assumes any legal liability or responsibility for the accuracy, completeness, or usefulness of any information, apparatus, product, or process disclosed, or represents that its use would not infringe privately owned rights. Reference herein to any specific commercial product, process, or service by trade name, trademark, manufacturer, or otherwise, does not necessarily constitute or imply its endorsement, recommendation, or favoring by the United States Government or any agency thereof. The views and opinions of authors expressed herein do not necessarily state or reflect those of the United States Government or any agency thereof.